Relationship between Prediction Skill of Surface Winds in Average of Weeks 1–4 and Interannual Variability over the Western Pacific and Indian Ocean

RAVI P. SHUKLA[a] AND J. L. KINTER[a,b]

[a] *Center for Ocean–Land–Atmosphere Studies, George Mason University, Fairfax, Virginia*
[b] *Department of Atmospheric, Oceanic, and Earth Sciences, George Mason University, Fairfax, Virginia*

(Manuscript received 18 September 2020, in final form 17 March 2021)

ABSTRACT: This study examines the possible relationship between predictions of weekly and biweekly averages of 10-m winds at 3-week lead time and interannual variability over the western Pacific and Indian Ocean (WP-IO) using Climate Forecast System version 2 (CFSv2) reforecasts for period 1979–2008. There is a large temporal correlation between forecasts and reanalyses for zonal, meridional, and total wind magnitudes at 10 m over most of WP-IO for the average of weeks 1 and 2 (W1 and W2) in reforecasts initialized in January (JIR) and May (MIR). The model has some correlations that exceed 95% confidence in some portions of WP-IO in week 3 (W3) but no skill in week 4 (W4) over most of the region. The model depicts prediction skill in the 14-day average of weeks 3–4 (W3–4) over portions of WP-IO, similar to the level of skill in W3. The amplitude of interannual variability (IAV) for 10-m winds in W1 of JIR and MIR is close to that in reanalyses. As lead time increases, the amplitude of IAV of 10-m winds gradually decreases over WP-IO in reforecasts, in contrast to behavior in reanalyses. The amplitude of IAV of predicted 10-m winds in W3–4 over WP-IO is equivalent to that in W3 and W4 in reforecasts. In contrast, the amplitude of IAV in W3–4 in January and May of the reanalysis is much smaller than IAV of W3 and W4. Therefore, one of the possible causes for prediction skill in W3–4 over subregions of WP-IO is due to a reduction of IAV bias in W3–4 in comparison to IAV bias in W3 and W4.

SIGNIFICANCE STATEMENT: Reliable prediction at the subseasonal time scale using a coupled land–atmospheric–ocean model is useful for making management decisions in agriculture and water management. This study explores a relationship between prediction skill of weekly average surface winds at lead times of 1–4 weeks and interannual variability over the western Pacific and Indian Ocean using the Climate Forecast System version 2 reforecasts during 1979–2008. The model has prediction skill in some subregions that exceeds 95% confidence in week 3 but no skill in week 4. Taking 14-day averages of weeks 3 and 4 produces forecasts whose skill is similar to that in week 3. There is a concurrent reduction in interannual variability during weeks 3 and 4 in reforecasts. A hypothesis is put forward that the subseasonal skill is related to the diminution of variability in the model.

KEYWORDS: Ensembles; Forecast verification/skill; Hindcasts; Climate models; Tropical variability

1. Introduction

The reliable prediction at the subseasonal time scale using the state-of-the-art coupled ocean–atmosphere–land general circulation models (CGCM) is very important because it fills the gap between medium-range weather prediction (up to 2 weeks) and seasonal mean prediction (e.g., NRC 2010; Koster et al. 2011; Vitart et al. 2012; Hoskins 2013; Robertson et al. 2015; DelSole et al. 2017; Black et al. 2017; Mariotti et al. 2020; Merryfield et al. 2020). A more detailed introduction to prediction at the subseasonal scale is provided in other recent papers (Shukla and Kinter 2016; Shukla et al. 2018, 2020). Reliable prediction at subseasonal time scales is very useful in agriculture, transportation, and water and energy resources management (e.g., White et al. 2017; Shukla and Kinter 2016).

The current state of weekly average prediction skill at lead times of 1–4 weeks has been evaluated using the global ensemble prediction systems (EPS) (e.g., Pegion and Sardeshmukh 2011; Shukla and Kinter 2016; Li and Robertson 2015; Weber and Mass 2017; Vigaud et al. 2017, 2018; Sun et al. 2018; Pegion et al. 2019). For example, Shukla and Kinter (2016) found that the prediction skill of significant wave height (SWH) anomalies in week-1 (W1) and week-2 (W2) averages is high over most of the western Pacific and Indian Ocean (WP-IO) region, and there is prediction skill in some subregions of the WP-IO at 3-week lead time (W3) that exceed 95% confidence. They examined January initialized reforecasts (JIR) and May initialized reforecasts (MIR) produced by applying wind forecasts from the National Centers for Environmental Prediction (NCEP) Climate Forecast System version 2 (CFSv2; Saha et al. 2014) to WAVEWATCH-III (WW3; Tolman 2009). Li and Robertson (2015) compared the prediction skill of precipitation at lead times up to 4 weeks in three global EPS, and they found that all models are skillful in W1, but dramatically decreased skill for W2 to week 4 (W4). They also found that forecasts with the European Centre for Medium-Range Weather Forecasts (ECMWF) forecast system are noticeably better in W3 and W4 than forecasts from the CFSv2 or the

Supplemental information related to this paper is available at the Journals Online website: https://doi.org/10.1175/WAF-D-20-0181.s1.

Corresponding author: Ravi P. Shukla, rshukla2@gmu.edu

DOI: 10.1175/WAF-D-20-0181.1

Japan Meteorological Agency (JMA) EPS. Vigaud et al. (2017) found that the forecast skill of weekly average precipitation in three EPS reforecast sets (ECMWF EPS, NCEP CFSv2 and China Meteorological Administration EPS) is higher in winter than summer, and decreases with lead time, after one week. Using EPS reforecasts, Sun et al. (2018) found large anomaly correlation in W1 precipitation, 2-m temperature, and 500-hPa height over North America that exceed 95% confidence. The above studies found that there are some subregions of North America in W3 that exceed 95% confidence.

Many previous studies have discussed the subseasonal prediction skill of 14-day means at 3-week lead time [weeks 3 and 4 average (W3–4)] using a global EPS (e.g., Hudson et al. 2011; DelSole et al. 2017; Black et al. 2017; Vigaud et al. 2017, 2018; Shukla et al. 2018; Sun et al. 2018; Wang and Robertson 2019; Pegion et al. 2019). Using CFSv2 reforecasts, DelSole et al. (2017) found anomaly correlation of W3–4 precipitation and temperature over some subregions of the contiguous United States that exceed 95% confidence. Using two global EPS (ECMWF and CFSv2), Wang and Robertson (2019) found correlation that exceed 95% confidence for W3–4 precipitation and 2-m temperature over the United States, with the ECMWF EPS having slightly higher prediction skill than CFSv2 EPS. Shukla et al. (2018) found temporal correlations that exceed 95% confidence for W3–4 SWH over subregions of the WP-IO in January and May. In general, prediction skill for W3–4 is similar to that of W3 and larger than that of W4. For example, Vigaud et al. (2018) found higher ranked probability skill score and reliability for rainfall in W3–4 over the East Africa–West Asia region compared to W3 or W4 forecasts for starts in February–April in a multimodal ensemble. Using EPS reforecasts, Sun et al. (2018) found that the anomaly correlation for W3–4 precipitation, 2-m temperature, and 500-hPa height over North America is similar to the anomaly correlation in W3 and higher than that in W4.

In this paper, a possible cause for higher subseasonal prediction skill in the 14-day mean of weeks 3 and 4 is explored in the WP-IO region. For this purpose, a set of 20-member ensemble CFSv2 reforecasts for the period 1979–2008 over the WP-IO region, initialized in January and May as in (Shukla et al. 2018), has been examined. The temporal anomaly correlation and interannual variability of 10-m zonal and meridional wind, and the magnitude of 10-m winds has been computed for W1, W2, W3, W4, and W3–4 over the WP-IO region in JIR and MIR during 1979–2008. The prediction skill of 10-m winds in the W3–4 over WP-IO is found to be similar to that of W3 and higher than that of W4 in both JIR and MIR for period 1979–2008. While the amplitude of interannual variability of 10-m wind is similar in W1–W4 in the ECMWF interim reanalysis (ERA-Interim; Dee et al. 2011), this variability decreases gradually from W1 to W4 in the reforecasts. We explore a possible relationship between subseasonal prediction skill in average of weeks 1–4 and interannual variability in the CFSv2 reforecasts over the WP-IO region.

This paper is organized as follows. Section 2 describes the model, experimental design, verification datasets and analysis method. Section 3 presents results of subseasonal prediction skill of zonal and meridional winds at 10 m in the Indo-Pacific region and explores a relationship between prediction skill and interannual variability in the JIR and MIR. A summary and discussion are given in section 4.

2. Model description, experimental design, and observational datasets

The coupled model used in this study is the NCEP CFSv2 (Saha et al. 2014), which is composed of interacting component models representing the atmosphere (spectral horizontal resolution of T126 and 64 vertical levels in a hybrid sigma-pressure coordinate), ocean [Geophysical Fluid Dynamics Laboratory (GFDL) Modular Ocean Model version 4–MOM4; Griffies et al. 2004], sea ice (Winton 2000), and land surface (Noah LSM; Ek et al. 2003). The GFDL MOM4 is configured for the global ocean with a horizontal grid of 0.5° × 0.5° poleward of 30°S/30°N and meridional resolution increasing gradually to 0.25° between 10°S and 10°N. Vertically, it has 40 levels in a z coordinate, with 27 levels within the upper 400 m and the maximum depth at approximately 4.5 km.

Details of JIR and MIR are described in Shukla et al. (2018, 2020). Briefly, the model data are 1-month reforecasts generated from the beginning of January (JIR) and the beginning of May (MIR) for 1979–2008 using four different sets of ocean initial conditions (OICs) namely, NCEP CFSR (Saha et al. 2010), NCEP Global Ocean Data Assimilation System (GODAS; Behringer 2005), European Centre for Medium-Range Weather Forecasts (ECMWF) Ocean Reanalysis System 3 (ORA-S3; Balmaseda et al. 2008), and ECMWF Comprehensive Modeling of the Earth System for Better Climate Prediction and Projection (COMBINE-NV; Balmaseda et al. 2013) with a slightly revised version of CFSv2 (Huang et al. 2015). The analysis region is a portion of the western Pacific and Indian Oceans (WP-IO; 80°E–180°, 60°S–40°N) with a grid resolution of 1° × 1°. The results discussed in the paper are based on the mean of the 16 ensemble members daily instantaneous values (0000 UTC) in both JIR and MIR. The ECMWF ERA-Interim (Dee et al. 2011) instantaneous fields at 0000 UTC for the 30-yr period (1979–2008) are used to verify the model output. We have employed JIR because the influence of ENSO is strongest and MJO is active at that time in the WP-IO region. MIR was chosen because monsoon circulation is in transition phase over the WP-IP. As indicated above, W1, W2, W3, and W4 for JIR are the averages of 1–7 January, 8–14 January, 15–21 January, and 22–28 January, respectively, and W3–4 is defined as the average of 15–28 January. A similar convention is adopted for MIR.

The statistical significance of correlation coefficient is measured using a Student's t test: given the sample size, correlation values for 90%, 95%, 98%, and 99% significance levels are 0.30, 0.35, 0.41, and 0.45, respectively.

3. Results

a. Weekly prediction skills of surface winds

To explore the relationship between prediction skill and interannual variability at lead times of W1, W2, W3, W4, and W3–4, the temporal anomaly correlation coefficient (TACC),

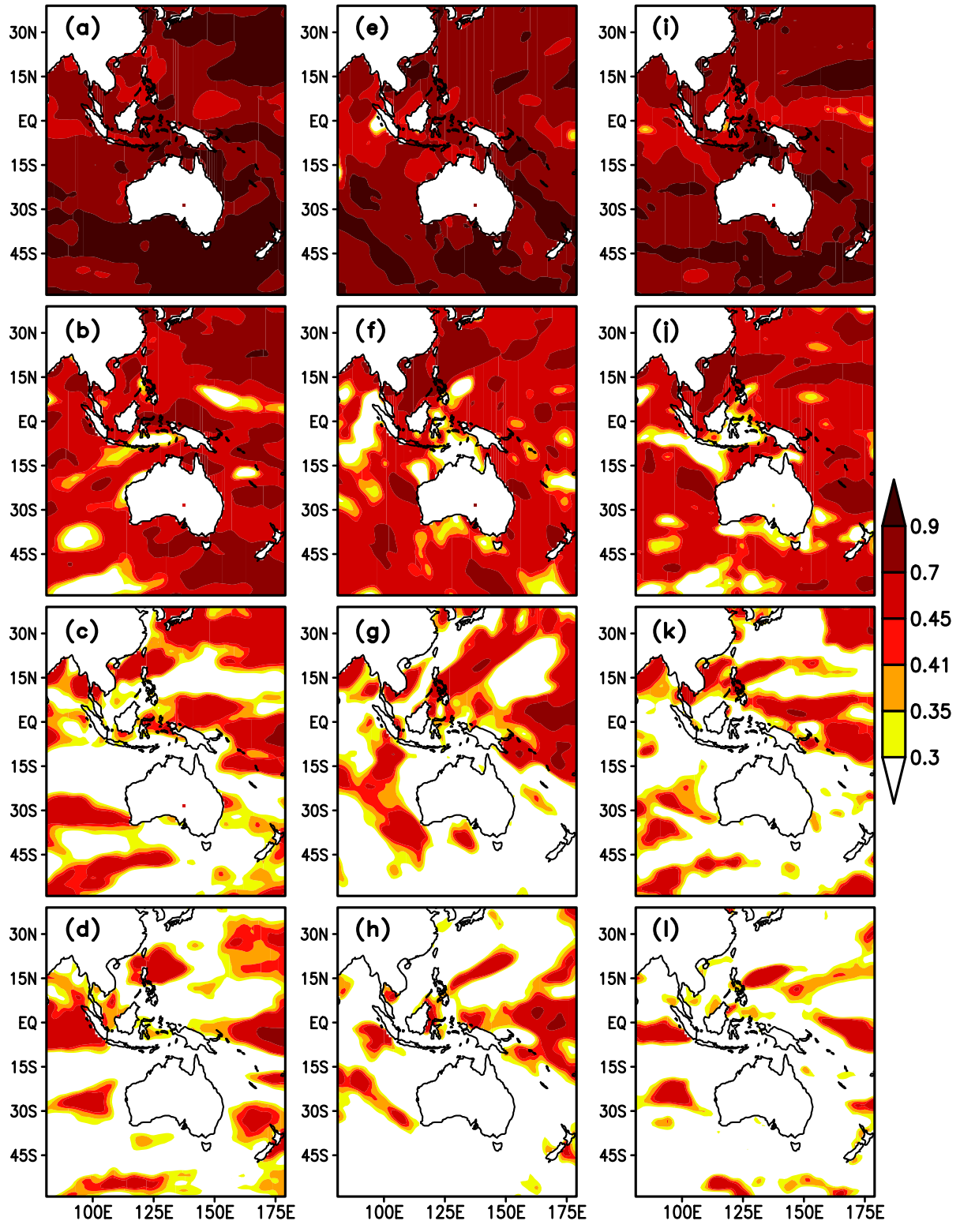

FIG. 1. Anomaly correlation skill of zonal winds at 10 m (U10m) at 0000 UTC between JIR and ERA-Interim in (a) W1, (b) W2, (c) W3, and (d) W4 for 1979–2008 over the western Pacific and Indian Oceans (WP-IO). Correlation coefficients (CC) contours are shown for 90% (CC = 0.30), 95% (CC = 0.35), 98% (CC = 0.41), and 99% (CC = 0.45) significance levels. (e)–(h) As in (a)–(d), but for meridional winds at 10 m (V10m). (i)–(l) As in (a)–(d), but for magnitude of 10-m winds (UV10m).

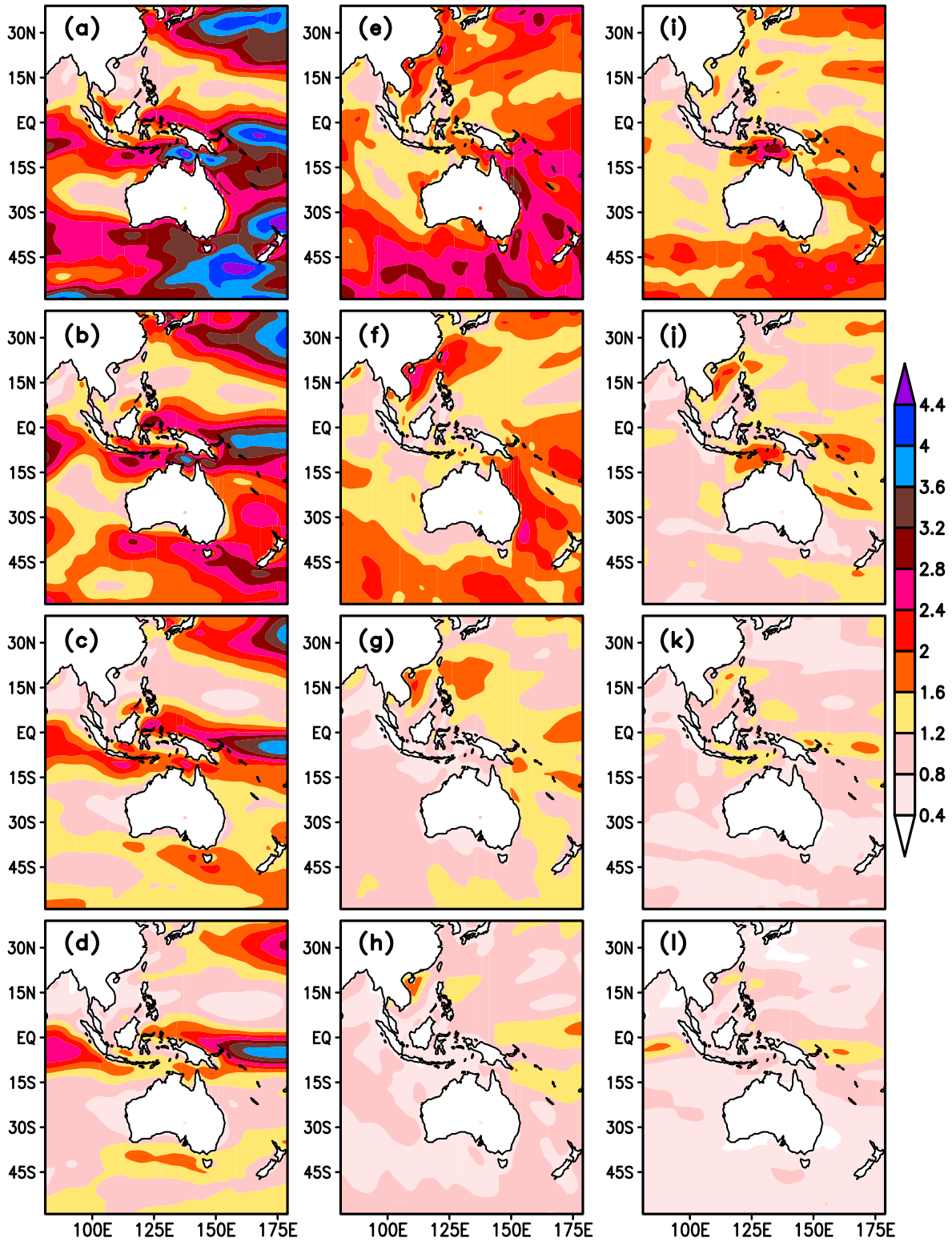

FIG. 2. The spatial distributions of interannual variability (IAV) of U10m in JIR at a lead time of (a) W1, (b) W2, (c) W3, and (d) W4 for 1979–2008 over the WP-IO. (e)–(h) As in (a)–(d), but for V10m. (i)–(l) As in (a)–(d), but for UV10m.

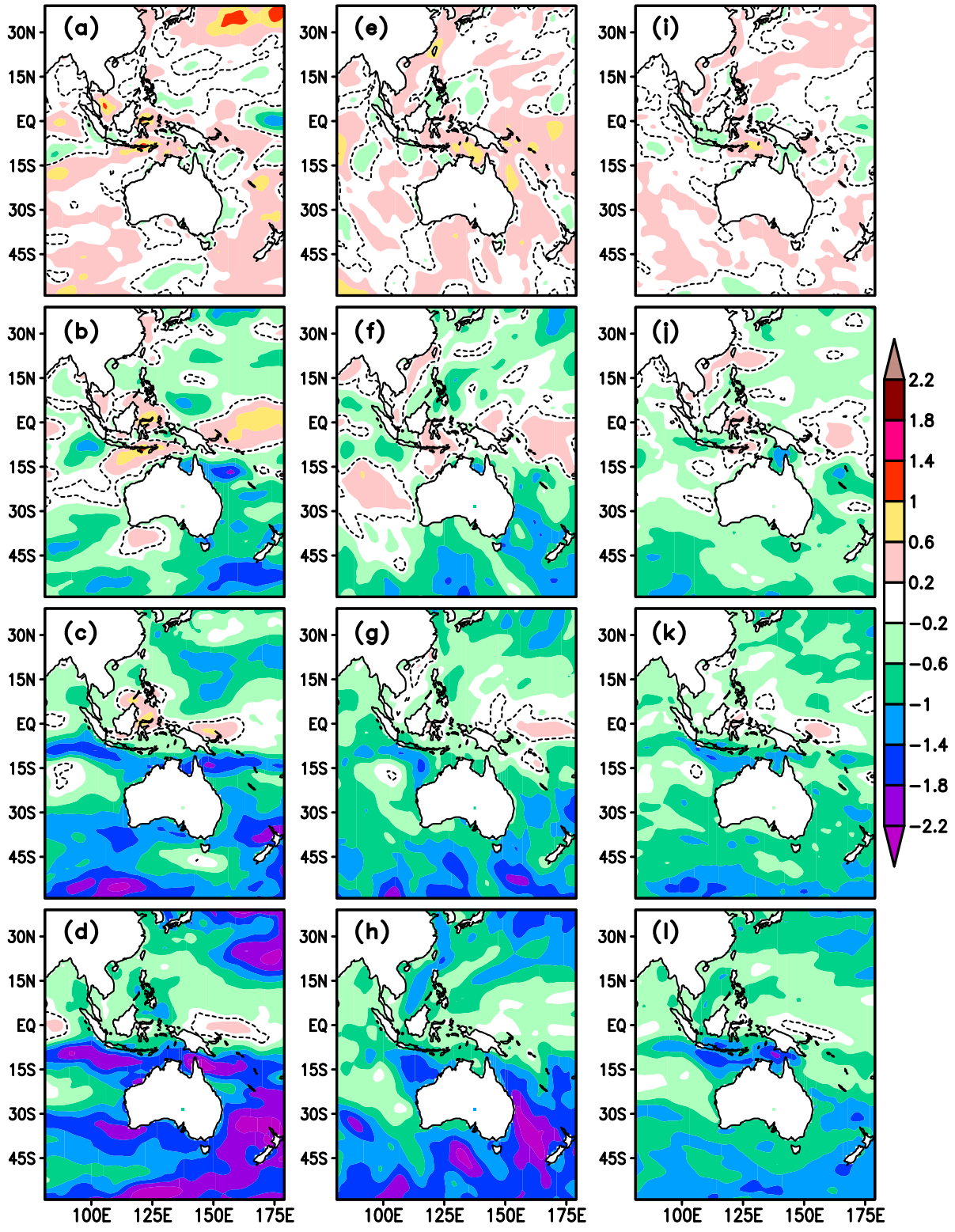

FIG. 3. The climatological bias of IAV of U10m in JIR relative to ERA-Intrimin in (a) W1, (b) W2, (c) W3, and (d) W4 for 1979–2008 over the WP-IO. (e)–(h) As in (a)–(d), but for V10m. (i)–(l) As in (a)–(d), but for UV10m.

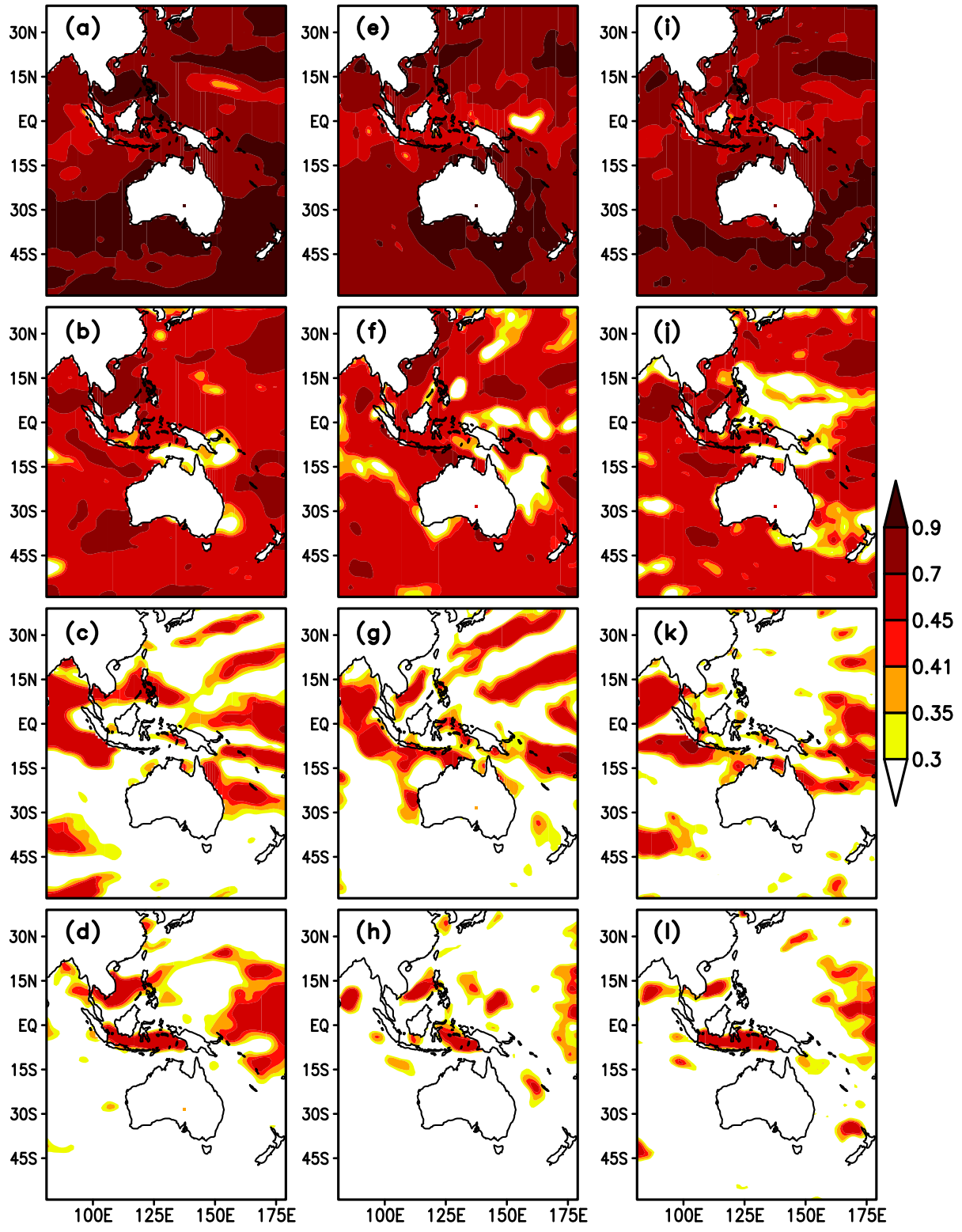

FIG. 4. Anomaly correlation skill of U10m at 0000 UTC between MIR and ERA-Interim in (a) W1, (b) W2, (c) W3, and (d) W4 for 1979–2008 over the WP-IO. Correlation coefficients contours are shown for 90% (CC = 0.30), 95% (CC = 0.35), 98% (CC = 0.41), and 99% (CC = 0.45) significance levels. (e)–(h) As in (a)–(d), but for V10m. (i)–(l) As in (a)–(d), but for UV10m.

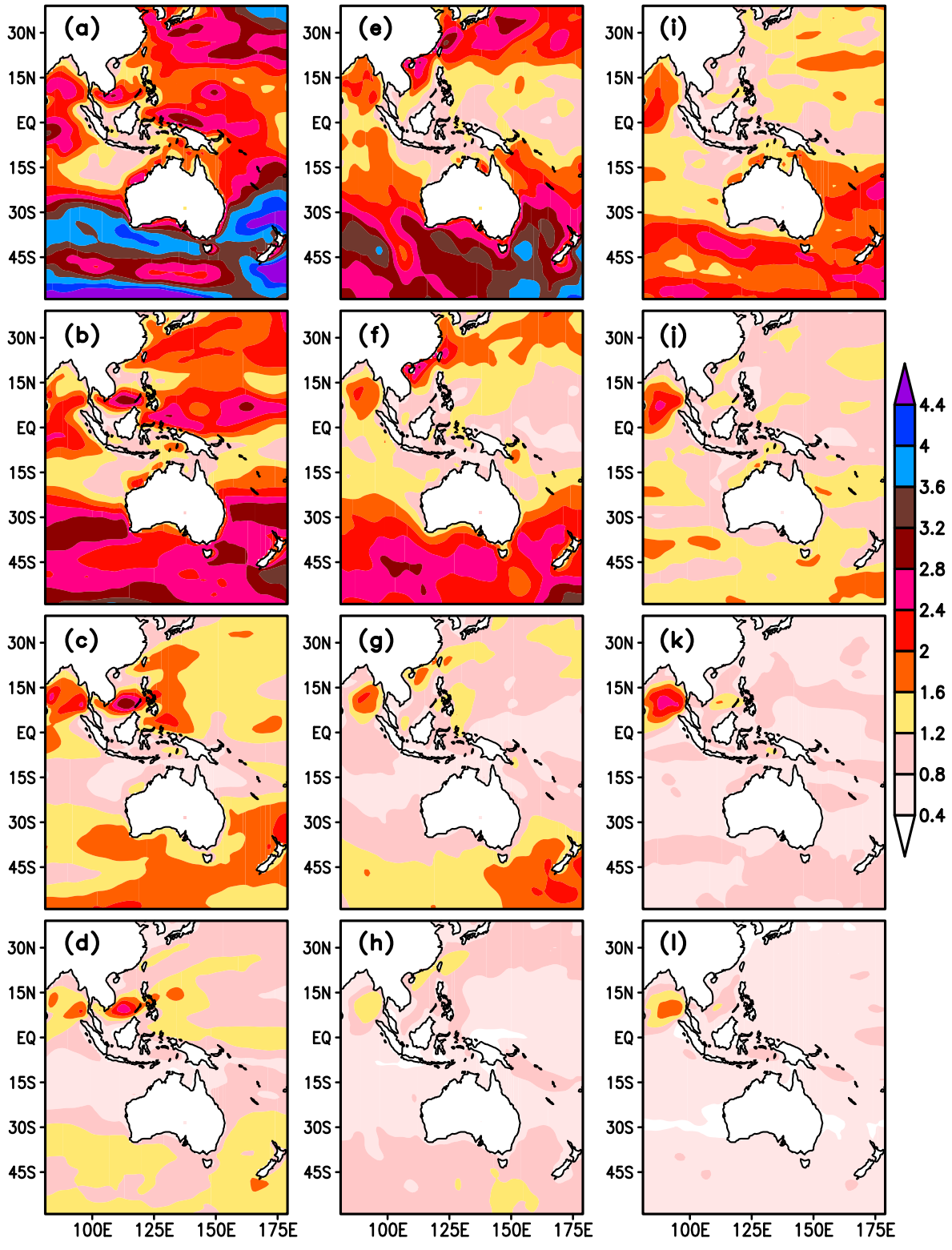

FIG. 5. The spatial distributions of IAV of U10m in MIR at a lead time of (a) W1, (b) W2, (c) W3, and (d) W4 for 1979–2008 over the WP-IO. (e)–(h) As in (a)–(d), but for V10m. (i)–(l) As in (a)–(d), but for UV10m.

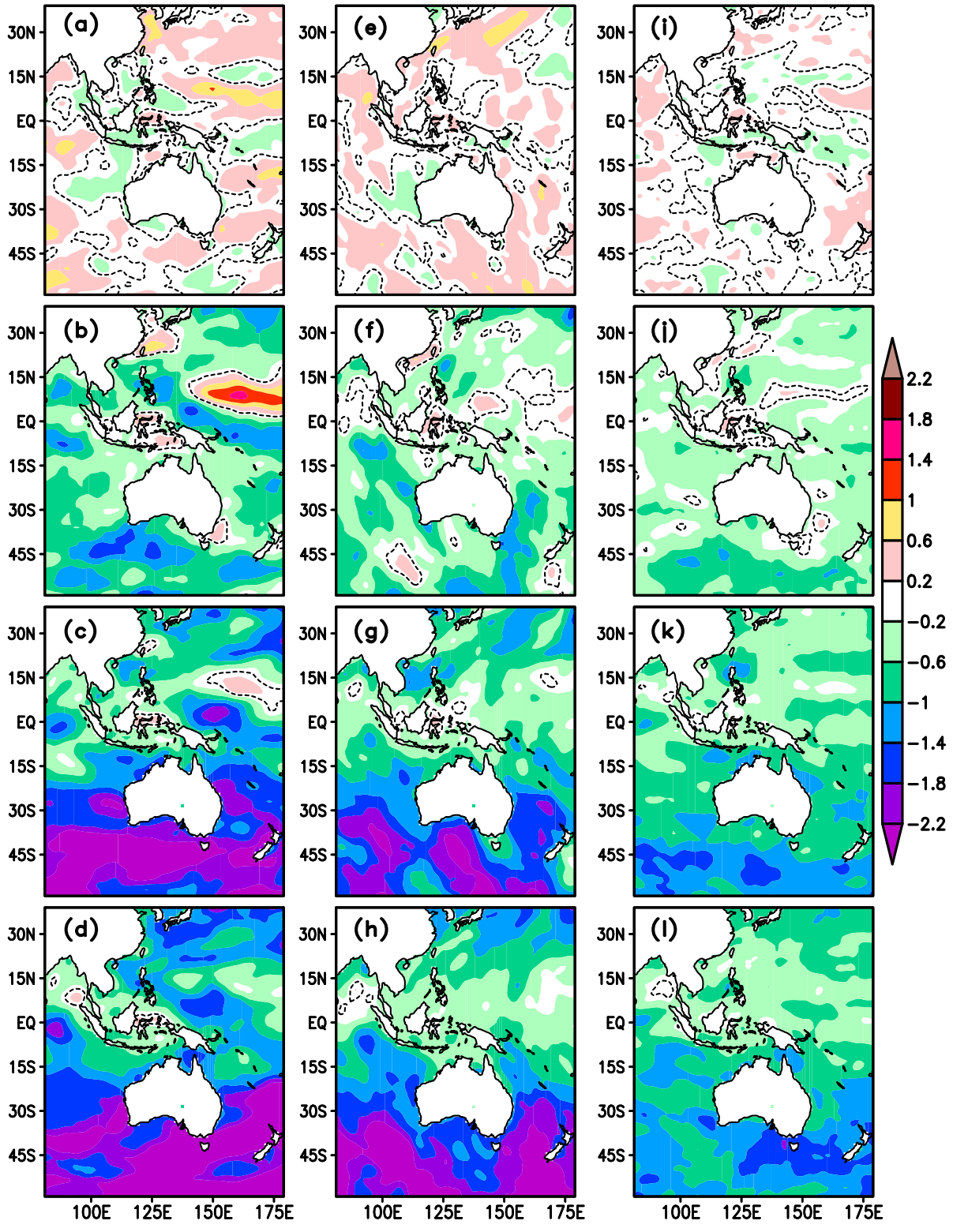

FIG. 6. The climatological bias of IAV of U10m in MIR relative to ERA-Intrimin in (a) W1, (b) W2, (c) W3, and (d) W4 for 1979–2008 over the WP-IO. (e)–(h) As in (a)–(d), but for V10m. (i)–(l) As in (a)–(d), but for UV10m.

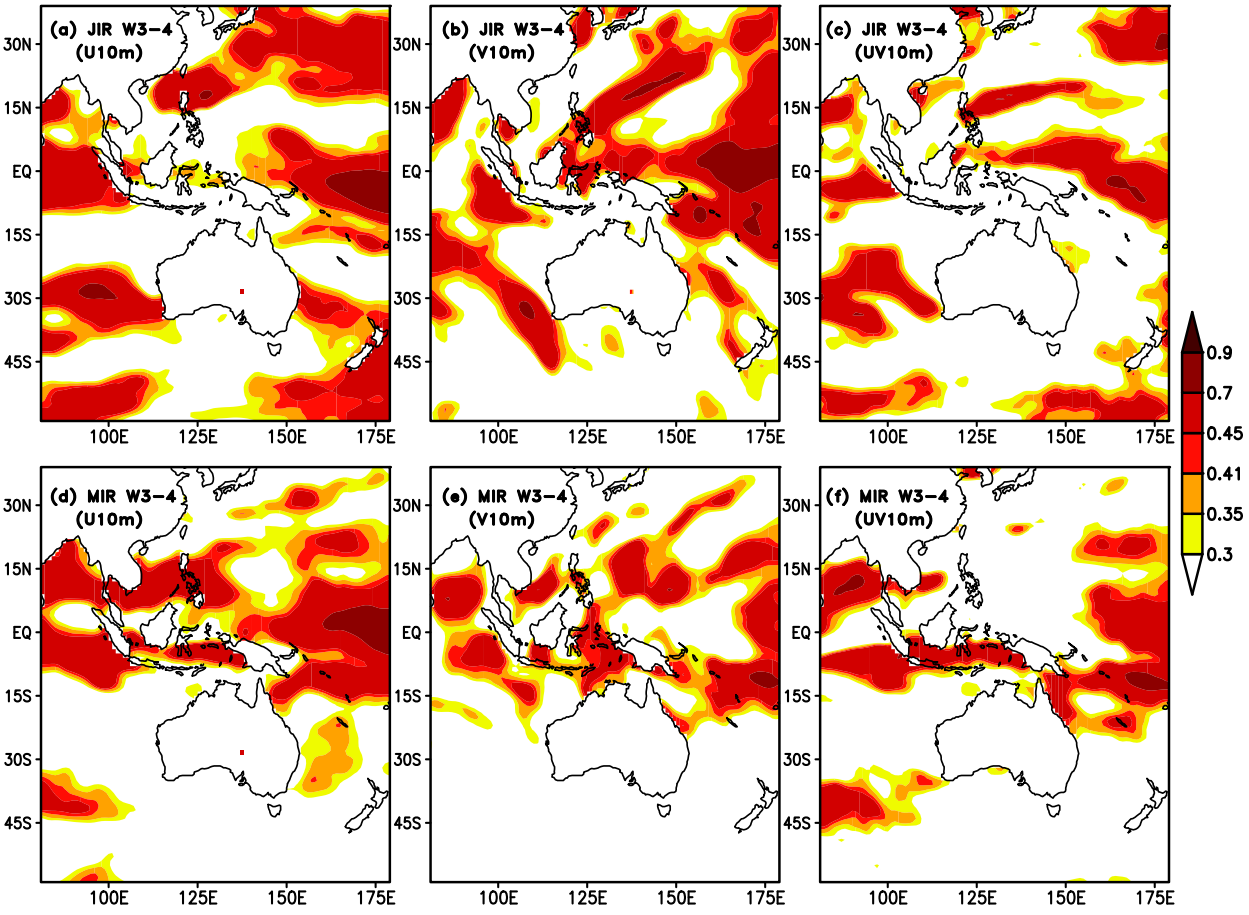

FIG. 7. (a) Anomaly correlation skill of U10m at 0000 UTC between JIR and ERA-Interim in average of weeks 3 and 4 (W3–4) for 1979–2008 over the WP-IO. Correlation coefficients contours are shown for 90% (CC = 0.30), 95% (CC = 0.35), 98% (CC = 0.41), and 99% (CC = 0.45) significance levels. (b) As in (a), but for V10m in JIR. (c) As in (a), but for UV10m in JIR. (d)–(f) As in (a)–(c), but for MIR for 1979–2008.

root-mean-square error (RMSE) and interannual variability (IAV) of zonal wind at 10 m (hereafter, U10m), meridional winds at 10 m (hereafter, V10m) and the magnitude of 10-m winds (hereafter, UV10m) are computed. A standard procedure has been employed to calculate the climatological mean of the ensemble mean of 16 members. For example, for JIR, the climatology was obtained based on 30-yr data of ensemble mean at lead times W1, W2, W3, W4, and W3–4 over the WP-IO region. For calculation interannual variability and anomaly correlation, the climatology for those reforecasts was removed in both JIR and MIR. The interannual variability (IAV) is the square root of the variance in reforecast and reanalysis. The TACC and RMSE are calculated between anomaly of 10-m winds in reforecasts and reanalysis over the WP-IO region.

1) WEEKLY PREDICTION SKILLS OF SURFACE WINDS IN JIR

Figure 1 depicts TACC for U10m (Figs. 1a–d), V10m (Figs. 1e–h), and UV10m (Figs. 1i–l) in JIR for W1, W2, W3, and W4 over the WP-IO. During the first two weeks, the TACC is large and that exceed 95% confidence over the entire WP-IO for all three variables. Portions of the WP-IO region have TACC that exceed 95% confidence for W3 over the equatorial western Pacific Ocean (150°E–180°, 15°S–10°N), Bay of Bengal (BOB), northwestern Pacific Ocean mainly between 25° and 40°N, and southern Indian Ocean (IO) (35°–25°S, 80°–120°E) for U10 (Fig. 1c), V10 (Fig. 1g) and UV10 (Fig. 1k). During W4, there are correlations that exceed 95% confidence in the equatorial western Pacific and equatorial IO for U10m (Fig. 1d) and in the equatorial western Pacific for V10m (Fig. 1h) but most of the subregions of the WP-IO do not exceed 95% confidence in W4 for UV10m (Fig. 1l). The RMSE is relatively low in W1 for U10m up to 1.9 m s^{-1} (Fig. S1a in the online supplemental material), V10m up to 1.0–1.6 m s^{-1} (Fig. S1e), and UV10m up to 1.0–1.3 m s^{-1} (Fig. S1i) in the equatorial western Pacific Ocean, Southern Ocean (SO), and equatorial IO. As lead time increases, the magnitude of RMSE increases over the WP-IO mainly in the SO in W3 and W4 for U10m up to 2.5–3.4 m s^{-1} (Figs. S1c,d), V10m up to 2.2–2.8 m s^{-1} (Figs. S1g,h), and UV10m up to 1.0–1.6 m s^{-1} (Figs. S1k,l).

Figure 2 shows IAV of U10m (Figs. 2a–d), V10m (Figs. 2e–h) and UV10m (Figs. 2i–l) in JIR. It is found that amplitude of IAV in W1 of JIR is up to 3.6–4.0 m s^{-1} for U10m (Fig. 2a), 2.4–2.8 m s^{-1} for V10m (Fig. 2b) and 1.6–2 m s^{-1} for the magnitude of UV10m mainly over the equatorial and northwestern Pacific,

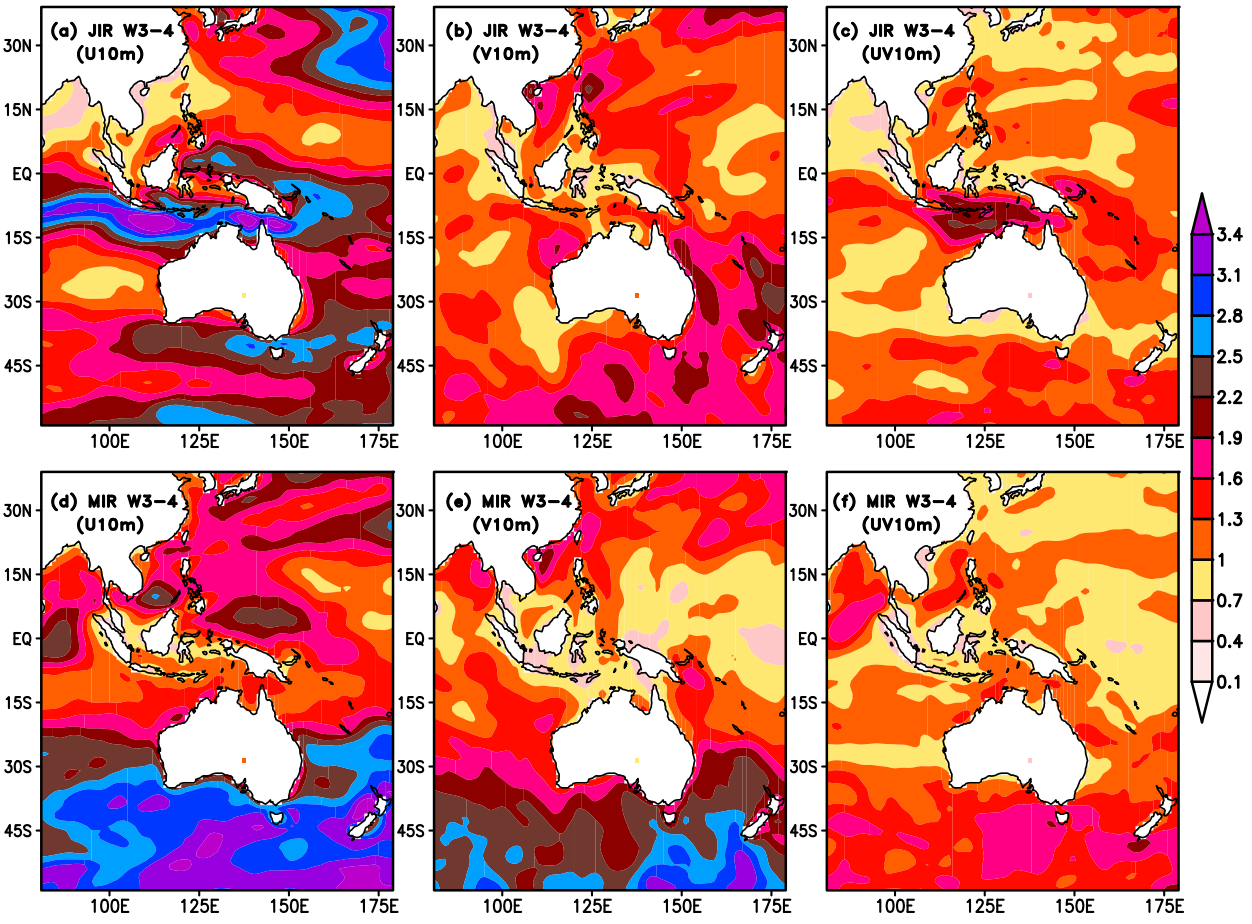

FIG. 8. (a) Root-mean-square error of U10m at 0000 UTC in average of W3–4 of JIR for 1979–2008 over the WP-IO. (b) As in (a), but for V10m in JIR. (c) As in (a), but for UV10U in JIR. (d)–(f) As in (a)–(c), but for MIR for 1979–2008.

SO, and equatorial IO, which is similar to that in January ERA-Interim reanalysis (Figs. S2a,e,i). As lead time increases, the magnitude of IAV decreases gradually mainly over the Southern Ocean in W3 and W4 of JIR (Fig. 2). The amplitude of IAV in W3 and W4 of JIR is up to 1.6–2.4 m s^{-1} for U10m over the equatorial western Pacific and IO (Figs. 2c,d), 0.8–1.6 m s^{-1} for V10m (Figs. 2g,h), and 0.8–1.2 m s^{-1} for UV10m (Figs. 2k,l). In contrast, the magnitude of IAV in the ERA-Interim reanalysis remains about the same for all weeks (from W1 to W4) in January for all three variables (Fig. S2). Therefore, there is relatively little IAV bias in W1 of JIR for all three variables (Figs. 3a,e,i). But, as lead time increases, the magnitude of IAV bias increases over the SO, mainly in W4 of JIR for U10m (Fig. 3d) up to −1.8 to −2.2 m s^{-1}, V10m (Fig. 3e) up to −1.4 to −1.8 m s^{-1} and magnitude of UV10m (Fig. 3l) up to −0.6 to −1.0 m s^{-1}.

2) WEEKLY PREDICTION SKILLS OF SURFACE WINDS IN MIR

For MIR, the TACC is large over the WP-IO region in W1 and W2 for U10m (Figs. 4a,b), V10m (Figs. 4e,f) and UV10m (Figs. 4i,j) that exceed 95% confidence except over the central-western Pacific in W2 for UV10m. There is skillful correlations that exceed 95% confidence in W3 over the southern BOB, equatorial IO and equatorial western Pacific (mainly 150°E–180°, 15°S–5°N) for all three variables (Figs. 4c,g,k). During W4 (Figs. 4d,h,l), correlation does not exceed 95% confidence almost everywhere except in the equatorial western Pacific for U10m. The RMSE is relatively small in W1 for U10m up to 1.0–1.6 m s^{-1} (Fig. S3a), V10m up to 1.0–1.9 m s^{-1} (Fig. S3e), and UV10m up to 0.7–1.3 m s^{-1} (Fig. S3i) in the SO, equatorial IO, and northern western Pacific. As lead time increases, the magnitude of RMSE increases mainly in the Southern Ocean in W3 and W4 for all three variables (Fig. S3). Overall, TACC (RMSE) is generally higher (lower) in the tropics (mainly 18°S–18°N) than the extratropical region (mainly, 20°–40°N and 60°–20°S) as noted before for significant wave height (SWH) over the IO-WP in the JIR and MIR (Shukla and Kinter 2016).

In MIR, the model IAV is large in W1 over the SO, equatorial and northern western Pacific, and equatorial IO for U10m up to 3.2–4.4 m s^{-1} (Fig. 5a), V10m up to 2.0–3.2 m s^{-1} (Fig. 5e) and UV10m up to 1.6–2.4 m s^{-1} (Fig. 5i), with amplitude very similar to that of the weekly means in the May ERA-Interim reanalysis (Figs. S4a,e,i), so that the bias is small in W1 of MIR for all three variables (Figs. 6a,e,i). As lead time increases, the magnitude of IAV decreases gradually in W3

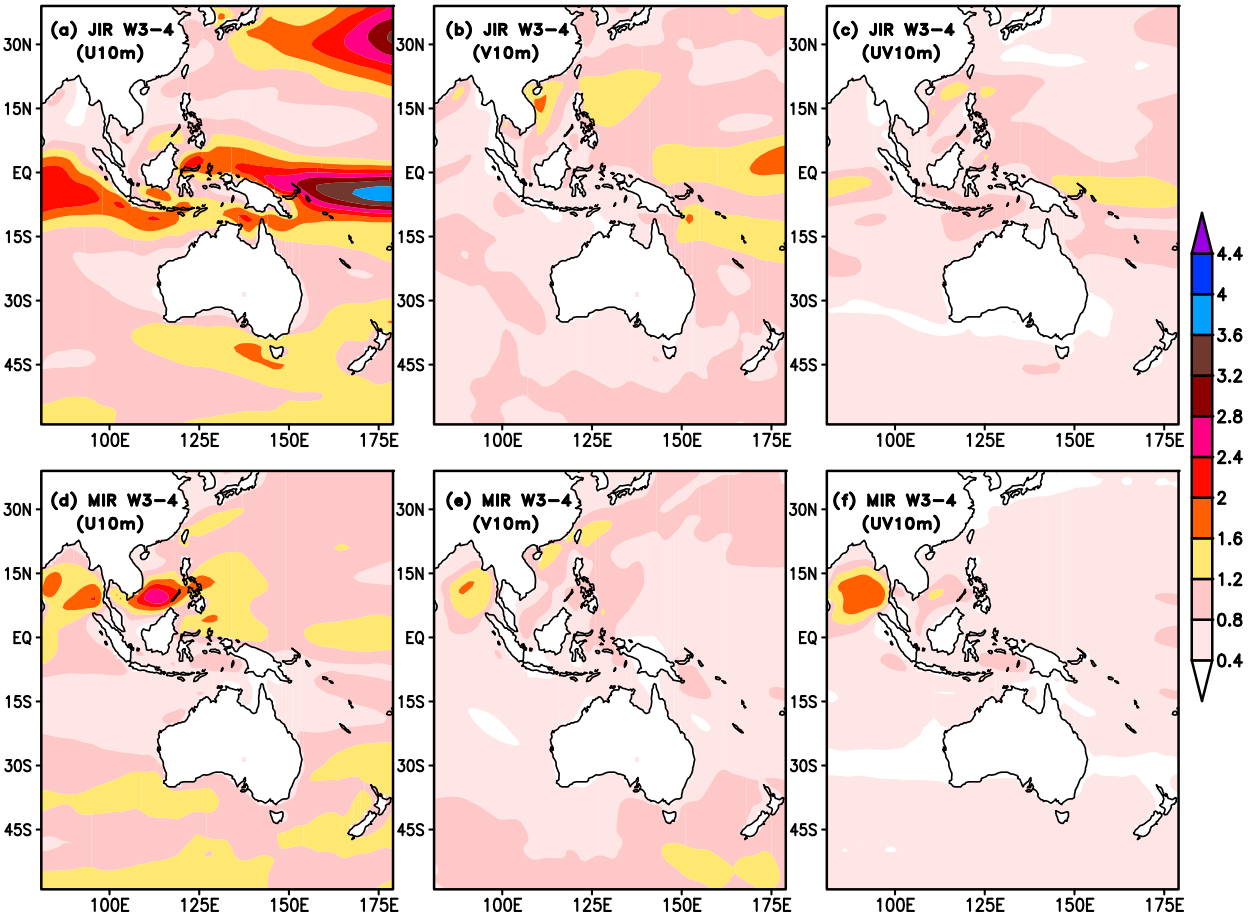

FIG. 9. (a) The spatial distributions of IAV of U10m in JIR at a lead time of average W3–4 for 1979–2008 over the WP-IO. (b) As in (a), but for V10m in JIR. (c) As in (a), but for UV10m in JIR. (d)–(f) As in (a)–(c), but for MIR for 1979–2008.

and W4 of MIR for all three variables (Fig. 5). The magnitude of IAV in all weekly means in May of the ERA-Interim reanalysis is about the same (Fig. S4). Therefore, the magnitude of IAV bias for all three variables is much larger over the SO in W4 compared to W1 of MIR (Fig. 6).

To summarize these results, in W1 and W2, reforecasts have large TACC that exceed 95% confidence and small IAV bias over most of the WP-IO in both January and May, for U10m, V10m, and UV10m. On the other hand, the model does not depict TACC that exceed 95% confidence in most of regions of the WP-IO in W4 and the IAV bias is large in W4, mainly in the Southern Ocean in January and May cases. Therefore, high correlation and low interannual variability bias coincide for U10m, V10m, and UV10m at lead times of weeks 1–4 in JIR and MIR. It is conceivable that if the IAV bias could be reduced in W3 and W4 in JIR and MIR, than skill of 10-m wind forecasts would be higher.

b. Biweekly prediction skills of surface winds

1) BIWEEKLY PREDICTION SKILLS OF SURFACE WINDS IN JIR

Figure 7 shows the W3–4 forecast skill (TACC) between U10m, V10m, and UV10m of JIR (MIR) and January (May) ERA-Interim reanalysis over the WP-IO. In January, there is correlations that exceed 95% confidence for U10m (Fig. 7a) over the equatorial and northern western Pacific, equatorial IO, and southern IO mainly in (80°–120°E, 42°–28°S). V10m forecasts (Fig. 7b) are skillful that exceed 95% confidence over central and northern western Pacific, southern BOB and southern IO mainly between (30°–15°S), and UV10m forecasts (Fig. 7c) are skillful that exceed 95% confidence over the equatorial western Pacific, southern BOB and southern IO mainly between (33°–15°S). The RMSE is relatively large in the SO, northern western Pacific, Maritime Continent, and equatorial IO mainly between (14°–6°S) for U10m up to 2.2–3.1 m s^{-1} (Fig. 8a), and over SO and northern western Pacific for V10m up to 1.3–1.9 m s^{-1} (Fig. 8b), and over the SO and Maritime Continent for UV10m up to 1.0–1.6 m s^{-1} (Fig. 8c).

The amplitude of IAV in the W3–4 of JIR is 1.2–2.0 m s^{-1} for U10m over the equatorial and northern western Pacific and equatorial IO (Fig. 9a), 0.8–1.6 m s^{-1} for V10m over the western Pacific (Fig. 9b), and 0.8–1.2 m s^{-1} for UV10m (Fig. 9c). It is necessary to mention that the amplitude and spatial structure of IAV in the W3–4 of JIR for U10m (Fig. 9a), V10m (Fig. 9b) and UV10m (Fig. 9c) is equivalent to amplitude and structure of IAV in the W3 and W4 of JIR

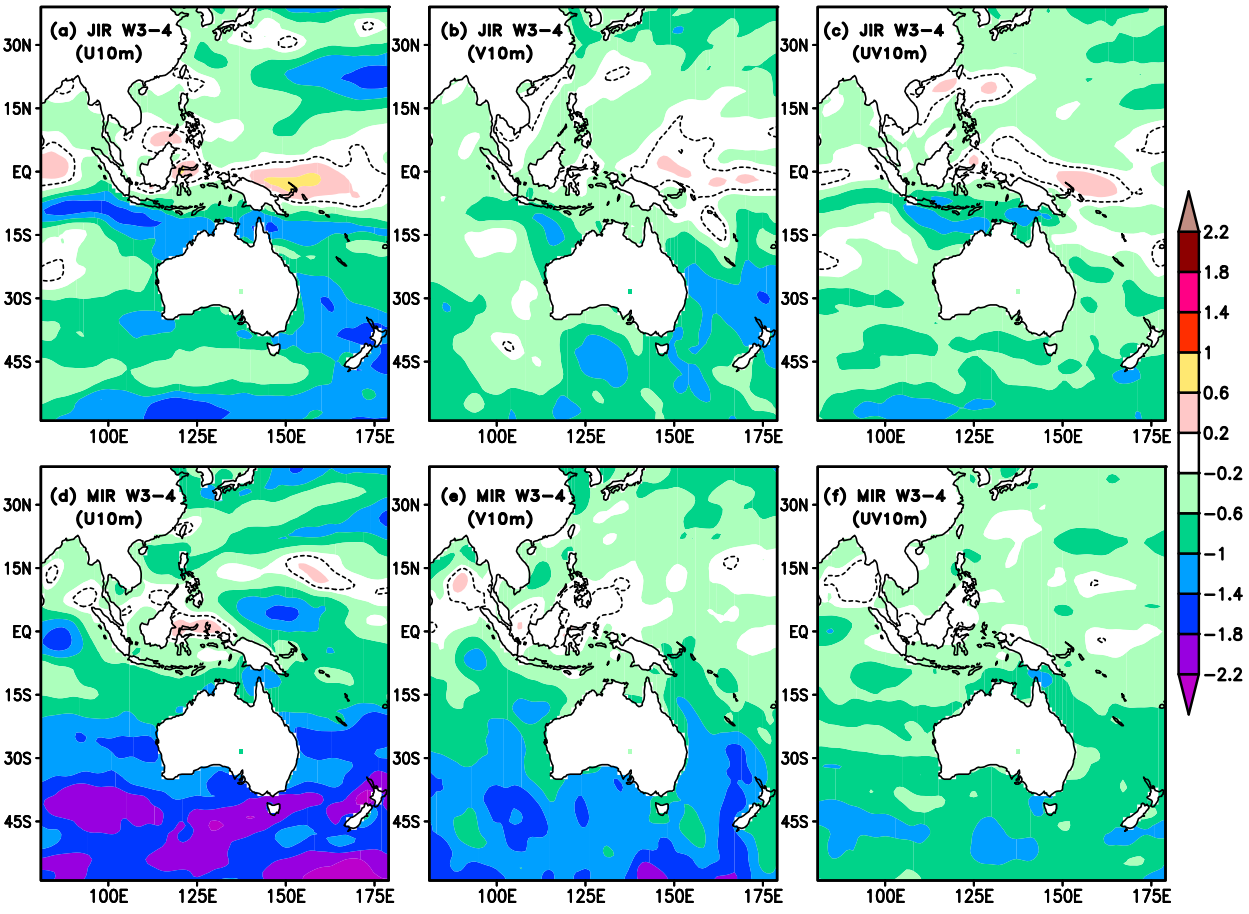

FIG. 10. (a) The climatological bias of IAV of U10m in JIR relative to ERA-Intrimin in average of W3–4 for 1979–2008 over the WP-IO. (b) As in (a), but for V10m in JIR. (c) As in (a), but for UV10m in JIR. (d)–(f) As in (a)–(c), but for MIR for 1979–2008.

for U10m (Figs. 2c,d), V10m (Figs. 2g,h) and UV10m (Figs. 2k,l). The amplitude of IAV in the average of W3–4 of January ERA-Interim reanalysis is 1.6–2.8 m s^{-1} for U10m over the central and northern western Pacific, SO and equatorial IO (Fig. S5a), 0.8–2.0 m s^{-1} for V10m over the SO, central and northern western Pacific (Fig. S5b), and 0.8–1.6 m s^{-1} for UV10m over the SO and equatorial IO (Fig. S5c). It is found the amplitude of IAV in W3–4 of January ERA-Interim reanalysis is much less than that of W3 and W4 of January ERA-Interim reanalysis for the U10m, V10m, and UV10m. Therefore, the amplitude of IAV bias in W3–4 (Figs. 10a–c) is smaller for all three variables than that for W3 (Figs. 3c,g,k) or W4 (Figs. 3d,h,l) in JIR over the WP-IO region.

2) BIWEEKLY PREDICTION SKILLS OF SURFACE WINDS IN MIR

In May, U10m forecasts (Fig. 7d) are skillful that exceed 95% confidence over the central western Pacific, BOB, South China Sea (SCS), equatorial IO, and Maritime Continent in W3–4. There is skillful correlation that exceed 95% confidence for V10m (Fig. 7e) in W3–4 over the northern BOB, Maritime Continent, SCS and western Pacific mainly regions (15°–2°S, 150°E–180°) and (5°–15°N, 125°–150°E). UV10m forecasts (Fig. 7f) are skillful that exceed 95% confidence over the northern BOB, IO mainly between (10°–5°S), Maritime Continent, western Pacific mainly between (10°S–10°N, 155°E–180°), and SO mainly between (45°–35°S). The model depicts relatively larger RMSE in W3–4 of MIR over the SO, northern western Pacific, BOB and SCS for U10m up to 1.6–3.1 m s^{-1} (Fig. 8d), and V10m up to 1.6–2.5 m s^{-1} (Fig. 8e), and over the SO and BOB for UV10m up to 1.0–1.6 m s^{-1} (Fig. 8f). Shukla et al. (2018, 2020) made a similar conclusion for SWH for the average of W3–4 over the IO-WP in JIR and MIR.

The amplitude of IAV in W3–4 of May (Figs. 9d–f) is generally smaller in the reforecasts (MIR) than in the ERA-Interim reanalysis (Figs. S5d–f), but the magnitude of bias in W3–4 for all three variables is smaller than that for W3 (Figs. 5c,g,k) or W4 (Figs. 5d,h,l). This is because the amplitude and spatial structure of W3–4 IAV in the reforecasts for MIR is similar to that in W3 and W4, whereas the IAV in the ERA-Interim reanalysis is much smaller in W3–4 than in either W3 or W4. It is found that taking a 14-day average of weeks 3 and 4 of January (May) ERA-Interim reanalysis for U10m, V10m and UV10m reduces the amplitude of IAV in the W3–4 compared to the 7-day averages in W3 and W4. We have also found that the IAV bias of SWH in W3–4 is less over most of region of

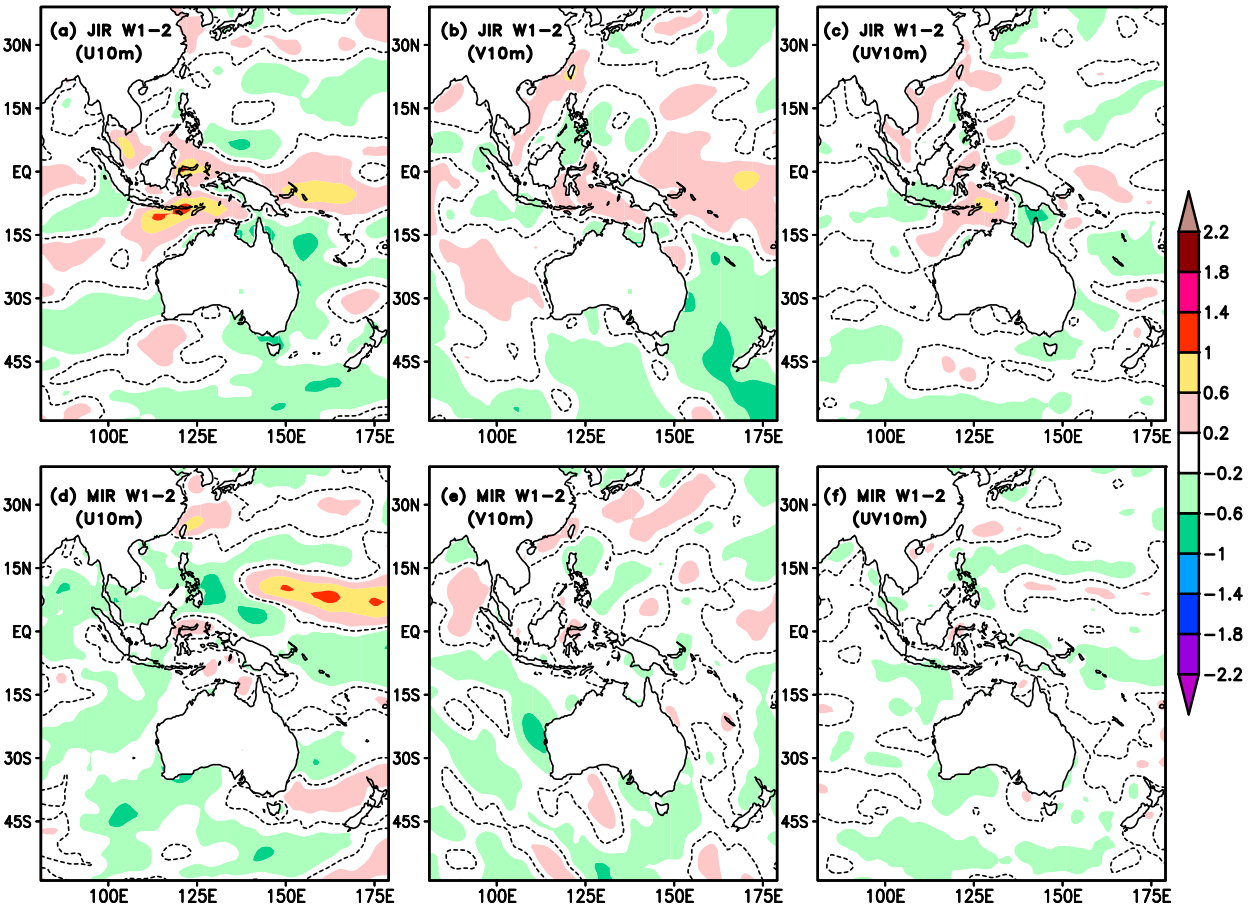

FIG. 11. (a) The climatological bias of IAV of U10m in JIR relative to ERA-Intrimin in average of W1–2 for 1979–2008 over the WP-IO. (b) As in (a), but for V10m in JIR. (c) As in (a), but for UV10m in JIR. (d)–(f) As in (a)–(c), but for MIR for 1979–2008.

WP-IO than the IAV bias of SWH in W3 and W4 in JIR and MIR (results not shown).

4. Summary and discussion

A relationship between subseasonal prediction skill and interannual variability of 10-m wind at lead times of average of weeks 1 to 4 has been analyzed over the WP-IO region using the coupled CFSv2 reforecasts in January and May cases during period 1979–2008. While the model is skillful prediction skill over most of the WP-IO region that exceed 95% confidence in W1 and W2, it is generally less skillful in W3 and W4, although there are subregions with useful anomaly correlation that exceed 95% confidence in W3 (e.g., equatorial and northern western Pacific Ocean, Bay of Bengal in January and southern BOB, equatorial IO, and equatorial western Pacific in May). For W4 there are only pockets of useful TACC that exceed 95% confidence, e.g., over the equatorial western Pacific and equatorial IO for U10m and the equatorial western Pacific for V10m in January. The RMSE is lower in W1 but as lead time increases, the amplitude of weekly mean RMSE increases mainly in the Southern Ocean.

The interannual variability of U10m, V10m, and UV10m over the WP-IO has nearly the same magnitude in reforecasts and the ERA-Interim reanalysis in W1 for both January and May cases. Therefore the IAV bias is relatively small in W1. As lead time increases, the amplitude of weekly average IAV decreases gradually in the WP-IO mainly over the Southern Ocean, especially in W3 and W4, while the IAV in the ERA-Interim reanalysis remains roughly the same over each 4-week period (January and May). This feature and the subsequent discussion hold for all three surface wind variables (U10, V10, and UV10). Therefore, there is much larger weekly average IAV bias in W3 and W4 as a result in JIR and MIR over the WP-IO region.

While the skill is more modest in the 14-day averages of W3–4, there is skillful TACC that exceed 95% confidence for U10m, V10m, and UV10m over the equatorial and northwestern Pacific Ocean, equatorial IO, southern BOB, and southern IO in JIR, and over the central western Pacific, BOB, South China Sea, equatorial IO, and Maritime Continent in MIR. The amplitude and spatial structure of IAV in the 14-day average of W3–4 of JIR and MIR is equivalent to the amplitude and structure of IAV in the 7-day means for W3 and W4 of JIR and MIR. In other words, the longer time (14-day) average produces IAV comparable in magnitude to the shorter (7-day) average in JIR and MIR. In contrast, the amplitude of IAV in

the 14-day mean W3–4 of January and May ERA-Interim reanalysis is much less than that of W3 or W4. That is, the longer time average reduces the variance in the ERA-Interim reanalysis. Therefore, the amplitude of IAV bias in W3–4 is smaller over the WP-IO than that for W3 or W4 of JIR and MIR.

The behavior in JIR and MIR at longer lead times (weeks 3–4) is different from the first two weeks. It is also found that the IAV of 10-m winds in the 14-day average of weeks 1 and 2 (W1–2) in JIR (Figs. S6a–c) and MIR (Figs. 6d–f) over the WP-IO is close to that in January (Figs. S7a–c) and May (Figs. S7d–f) ERA-Interim reanalysis for period 1979–2008. Therefore, the model has less IAV bias for U10m, V10m, and UV10m in W1–2 over the WP-IO in JIR (Figs. 11a–c) and MIR (Figs. 11d–f). The TACC for 10-m winds in 14-day means in W1–2 of WP-IO in JIR (Figs. S8a–c) and MIR (Figs. S8d–f) is similar to that in W1 in JIR (Figs. 1a,e,i) and MIR (Figs. 4a,e,i). It is necessary to mention that IAV bias of U10m, V10m, and UV10m for W3–4 in JIR and MIR is larger than that for W1–2 over the WP-IO for period 1979–2008, therefore, prediction skill of 10-m winds for W3–4 in JIR and MIR over the WP-IO is lower than in W1–2.

There is no TACC that exceed 95% confidence over most of the WP-IO region in W4 in January or May, but the correlation is larger in some subregions of WP-IO in the 14-day average of W3–4. The places where TACC is exceeding 95% confidence in W3–4 coincide with the places where the TACC is larger in W3. Therefore, the skill of W3–4 largely results from the skill of W3 in these places.

The results of this analysis support the conjecture that the model deficiency in maintaining the variance of near-surface wind leads to a diminution of skill in temporal averages. This deficiency is most acute at the weekly average time scale and is readily apparent in comparison of forecast statistics at lead times of 1–2 weeks with the same statistics at lead times of 3–4 weeks. There is also an indication that the presence of skill in the W3–4 reforecasts where there is no correlations that exceed 95% confidence in W4 may be a result of the diminution of IAV bias in W3–4. The results of this paper provide the importance of interannual variability of 10-m winds in the subseasonal prediction in the state-of-the-art coupled general circulation model reforecasts.

Acknowledgments. Funding for this research work was provided by grants from the National Science Foundation (1338427), the National Oceanic and Atmospheric Administration (NA14OAR4310160), and the National Aeronautics and Space Administration (NNX14AM19G). The computations were made on the Extreme Science and Engineering Discovery Environment (XSEDE) high-performance computing platform (Towns et al. 2014), and the computational resources are gratefully acknowledged. The authors are grateful to two anonymous reviewers for their constructive comments and suggestions, which improved the quality of the manuscript.

Data availability statement. We would like to share our model outputs that support the findings of this study to scientific community through Zenodo (DOI: 10.5281/zenodo.4035103).

REFERENCES

Balmaseda, M. A., A. Vidard, and D. L. T. Anderson, 2008: The ECMWF Ocean Analysis System: ORA-S3. *Mon. Wea. Rev.*, **136**, 3018–3034, https://doi.org/10.1175/2008MWR2433.1.

——, K. Mogensen, and A. T. Weaver, 2013: Evaluation of the ECMWF ocean reanalysis system ORAS4. *Quart. J. Roy. Meteor. Soc.*, **139**, 1132–1161, https://doi.org/10.1002/qj.2063.

Behringer, D. W., 2005: The Global Ocean Data Assimilation System (GODAS) as NCEP. *11th Symp. on Integrated Observing and Assimilation Systems for the Atmosphere, Oceans, and Land Surface*, San Antonio, TX, Amer. Meteor. Soc., 3.3, https://ams.confex.com/ams/87ANNUAL/webprogram/Paper119541.html.

Black, J., N. C. Johnson, S. Baxter, S. B. Feldstein, D. S. Harnos, and M. L. L'Heureux, 2017: The predictors and forecast skill of Northern Hemisphere teleconnection patterns for lead times of 3–4 weeks. *Mon. Wea. Rev.*, **145**, 2855–2877, https://doi.org/10.1175/MWR-D-16-0394.1.

Dee, D. P., and Coauthors, 2011: The ERA-Interim reanalysis: Configuration and performance of the data assimilation system. *Quart. J. Roy. Meteor. Soc.*, **137**, 553–597, https://doi.org/10.1002/qj.828.

DelSole, T., L. Trenary, M. K. Tippett, and K. Pegion, 2017: Predictability of weeks 3–4 average temperature and precipitation over the contiguous United States. *J. Climate*, **30**, 3499–3512, https://doi.org/10.1175/JCLI-D-16-0567.1.

Ek, M., K. E. Mitchell, Y. Lin, E. Rogers, P. Grunmann, V. Koren, G. Gayno, and J. D. Tarpley, 2003: Implementation of Noah land surface model advances in the National Centers for Environmental Prediction operational mesoscale Eta model. *J. Geophys. Res.*, **108**, 8851, https://doi.org/10.1029/2002JD003296.

Griffies, S. M., M. J. Harrison, R. C. Pacanowski, and A. Rosati, 2004: Technical guide to MOM4. GFDL Ocean Group Tech. Rep. 5, 371 pp., http://www.gfdl.noaa.gov/fms.

Hoskins, B., 2013: The potential for skill across the range of the seamless weather-climate prediction problem: A stimulus for our science. *Quart. J. Roy. Meteor. Soc.*, **139**, 573–584, https://doi.org/10.1002/qj.1991.

Huang, B., and Coauthors, 2015: Climate drift of AMOC, North Atlantic salinity and Arctic sea ice in CFSv2 decadal predictions. *Climate Dyn.*, **44**, 559–583, https://doi.org/10.1007/s00382-014-2395-y.

Hudson, D., O. Alves, H. H. Hendon, and A. G. Marshall, 2011: Bridging the gap between weather and seasonal forecasting: Intraseasonal forecasting for Australia. *Quart. J. Roy. Meteor. Soc.*, **137**, 673–689, https://doi.org/10.1002/qj.769.

Koster, R. D., S. P. P. Mahanama, T. J. Yamada, G. Balsamo, A. A. Berg, M. Boisserie, and Z. Guo, 2011: The second phase of the global land–atmosphere coupling experiment: Soil moisture contributions to subseasonal forecast skill. *J. Hydrometeor.*, **12**, 805–822, https://doi.org/10.1175/2011JHM1365.1.

Li, S., and A. W. Robertson, 2015: Evaluation of submonthly precipitation forecast skill from global ensemble prediction systems. *Mon. Wea. Rev.*, **143**, 2871–2889, https://doi.org/10.1175/MWR-D-14-00277.1.

Mariotti, A., and Coauthors, 2020: Windows of opportunity for skillful forecasts subseasonal to seasonal and beyond. *Bull. Amer. Meteor. Soc.*, **101**, E608–E625, https://doi.org/10.1175/BAMS-D-18-0326.1.

Merryfield, W. J., and Coauthors, 2020: Current and emerging developments in subseasonal to decadal prediction. *Bull.*

Amer. Meteor. Soc., **101**, E869–E896, https://doi.org/10.1175/BAMS-D-19-0037.1.

National Research Council, 2010: *Assessment of Intraseasonal to Interannual Climate Prediction and Predictability*. National Academic Press, 192 pp., https://doi.org/10.17226/12878.

Pegion, K., and P. D. Sardeshmukh, 2011: Prospects for improving subseasonal predictions. *Mon. Wea. Rev.*, **139**, 3648–3666, https://doi.org/10.1175/MWR-D-11-00004.1.

——, and Coauthors, 2019: The Subseasonal Experiment (SubX): A multimodel subseasonal prediction experiment. *Bull. Amer. Meteor. Soc.*, **100**, 2043–2060, https://doi.org/10.1175/BAMS-D-18-0270.1.

Robertson, A. W., A. Kumar, M. Peña, and F. Vitart, 2015: Improving and promoting subseasonal to seasonal prediction. *Bull. Amer. Meteor. Soc.*, **96**, ES49–ES53, https://doi.org/10.1175/BAMS-D-14-00139.1.

Saha, S., and Coauthors, 2010: The NCEP Climate Forecast System Reanalysis. *Bull. Amer. Meteor. Soc.*, **91**, 1015–1057, https://doi.org/10.1175/2010BAMS3001.1.

——, and Coauthors, 2014: The NCEP Climate Forecast System version 2. *J. Climate*, **27**, 2185–2208, https://doi.org/10.1175/JCLI-D-12-00823.1.

Shukla, R. P., and J. L. Kinter, 2016: Subseasonal prediction of significant wave heights over the western Pacific and Indian Ocean region. *Wea. Forecasting*, **31**, 1733–1751, https://doi.org/10.1175/WAF-D-16-0078.1.

——, ——, and C.-S. Shin, 2018: Sub-seasonal prediction of significant wave heights over the western Pacific and Indian Oceans. Part II: The impact of ENSO and MJO. *Ocean Modell.*, **123**, 1–15, https://doi.org/10.1016/j.ocemod.2018.01.002.

——, ——, and ——, 2020: Corrigendum to ''Sub-seasonal prediction of significant wave heights over the Western Pacific and Indian Oceans. Part II: The impact of ENSO and MJO.'' *Ocean Modell.*, **152**, 101647, https://doi.org/10.1016/j.ocemod.2020.101647.

Sun, S., B. W. Green, R. Bleck, and S. G. Benjamin, 2018: Subseasonal forecasting with an icosahedral, vertically quasi-Lagrangian coupled model. Part II: Probabilistic and deterministic forecast skill. *Mon. Wea. Rev.*, **146**, 1619–1639, https://doi.org/10.1175/MWR-D-18-0007.1.

Tolman, H. L., 2009: User manual and system documentation of WAVEWATCH III TM version 3.14. NOAA/NWS/NCEP/MMAB Tech. Note 276, 194 pp.

Towns, J., and Coauthors, 2014: XSEDE: Accelerating scientific discovery. *Comput. Sci. Eng.*, **16**, 62–74, https://doi.org/10.1109/MCSE.2014.80.

Vigaud, N., A. W. Robertson, and M. K. Tippett, 2017: Multimodel ensembling of subseasonal precipitation forecasts over North America. *Mon. Wea. Rev.*, **145**, 3913–3928, https://doi.org/10.1175/MWR-D-17-0092.1.

——, M. K. Tippett, and A. W. Robertson, 2018: Probabilistic skill of subseasonal precipitation forecasts for the East Africa–West Asia sector during September–May. *Wea. Forecasting*, **33**, 1513–1532, https://doi.org/10.1175/WAF-D-18-0074.1.

Vitart, F., A. W. Robertson, and D. L. T. Anderson, 2012: Subseasonal to seasonal prediction project: Bridging the gap between weather and climate. *WMO Bull.*, **61**, 23–28.

Wang, L., and A. W. Robertson, 2019: Week 3–4 predictability over the United States assessed from two operational ensemble prediction systems. *Climate Dyn.*, **52**, 5861–5875, https://doi.org/10.1007/s00382-018-4484-9.

Weber, N. J., and C. F. Mass, 2017: Evaluating CFSv2 subseasonal forecast skill with an emphasis on tropical convection. *Mon. Wea. Rev.*, **145**, 3795–3815, https://doi.org/10.1175/MWR-D-17-0109.1.

White, C. J., and Coauthors, 2017: Potential applications of subseasonal-to-seasonal (S2S) predictions. *Meteor. Appl.*, **24**, 315–325, https://doi.org/10.1002/met.1654.

Winton, M., 2000: A reformulated three-layer sea ice model. *J. Atmos. Oceanic Technol.*, **17**, 525–531, https://doi.org/10.1175/1520-0426(2000)017<0525:ARTLSI>2.0.CO;2.